

Impact of the 125 GeV Higgs boson on the singlet fermion dark matter searches at the LHC

P. Ko,^{1,*} Gang Li,^{2,†} and Jinmian Li^{1,‡}

¹*School of Physics, Korea Institute for Advanced Study, 85 Hoegiro, Seoul 02455, Korea*

²*Department of Physics, National Taiwan University, Taipei 10617, Taiwan*

(Dated: April 23, 2022)

Abstract

The search for singlet fermion dark matter at high-energy colliders is commonly analyzed with a singlet scalar mediator, which however violates the standard model (SM) gauge invariance, renormalizability and unitarity. These problems can be cured by introducing a mixing between the singlet scalar s and the SM Higgs boson h . Thus one has to consider two scalar mediators h_1 and h_2 , where h_1 is identified as the discovered 125 GeV Higgs boson. As a specific example, we consider the dark matter (DM) search in the $t\bar{t} + \cancel{E}_T$ channel. According to the masses of dark matter and two scalar mediators, we classify the process into four cases. By investigating the total cross sections and differential distributions, we find that the contribution of the 125 GeV Higgs boson h_1 cannot be neglected in all cases and can even dominate once h_1 is on-shell in dark matter production. Further, we study the impact of h_1 on the LHC bounds of dark matter searches in the hadronic and semileptonic channels with the integrated luminosity of 36 fb^{-1} . Finally we make a brief comment that h_1 should be also considered in the vector DM search at high-energy colliders.

* pko@kias.re.kr

† gangli@phys.ntu.edu.tw

‡ jmli@kias.re.kr

I. INTRODUCTION

The framework of the simplified model [1, 2] (see also recent reports [3, 4]) has been widely used in studying the dark matter (DM) phenomenology at colliders, where the interaction energy scale can be much higher than the new physics scale so that the effective field theory approach is no longer valid [5–9]. In the simplified model for singlet fermion DM, a singlet scalar S is introduced, and its interaction with the standard model (SM) quarks and the fermionic DM χ are assumed to be described by the following Lagrangian [1, 2]:

$$\mathcal{L}_S = - \sum_q g_q \frac{m_q}{v} \bar{q}qS - g_\chi \bar{\chi}\chi S, \quad (1.1)$$

where $q(= u, d, s, c, b, t)$ are the SM quarks and $v = 246$ GeV. The couplings g_q and g_χ are usually chosen as $g_q = g_\chi = 1 - 5$ [2, 10] for simplicity and to guarantee a sufficient DM production rate at colliders. Since the coupling of the mediator to a heavier flavor is stronger, the DM production is dominated by the gluon fusion process with top quark involved at the Large Hadron Collider (LHC). Then, DM can be searched through the mono-jet signature [11, 12] with the top quark in the loop or through the production in association with top quark(s). Although the process of DM in association with a top quark pair or single top quark has a small production cross section, it can provide cleaner signals and more information on the nature of DM and the interaction form and has been studied extensively in the literature [2, 10, 13–17]. Especially, in Ref. [10] the $t\bar{t} + \cancel{E}_T$ signature is explored in the simplified model in a comprehensive way and is compared to the sensitivity with mono-jet signature as well as those without DM in the final state. In Refs. [13, 14], it is found that the LHC search sensitivity can be significantly improved if one also includes DM production in association with a single top quark. In fact, recent experimental results at the LHC [18–21] already show that the $t\bar{t} + \cancel{E}_T$ channel has a comparable sensitivity with the mono-jet channel. Moreover, the shapes of angular separations between the two leptons from top quark decays are found to be not only useful in resolving the coupling among the mediator and SM quark [2, 15, 16] but also helpful in distinguishing DM spins [17].

However, one can easily find that the Lagrangian (1.1) is not gauge invariant under the SM gauge transformations, since the SM left-handed quarks are in $SU(2)$ doublets while right-handed ones are singlets. In order that a singlet fermion DM can couple to SM particles in a renormalizable and gauge-invariant way, an economic way is to introduce a mixing between

the singlet scalar s with the SM Higgs boson after the electroweak symmetry breaking. As a result, there will be two physical scalar states (h_1 and h_2) mediating the SM and DM interactions. These two scalars are identified as the 125 GeV Higgs boson and a second scalar boson that can be either lighter or heavier than 125 GeV [22–24], respectively. These two scalar bosons also appear in the Higgs portal vector dark matter (VDM) model [25].

The main phenomenological differences between the gauge-invariant Higgs portal DM models and the simplified model (1.1) originating from the existence of the 125 GeV Higgs boson has been discussed in Refs. [26–28], and references therein. Especially, in Ref. [27] we have found that the interference effect between two mediators can affect the LHC exclusion bounds considerably in some parameter space, which was already reflected in Ref. [26] to some extent.

In this work, we will investigate the impact of h_1 (with the mass of 125 GeV) in the singlet fermionic DM (SFDM) model on the sensitivity of the LHC search for $t\bar{t} + \cancel{E}_T$. Depending on the masses of DM and mediators, four different cases (named Case A,B,C and D) shall be classified and discussed. The collider bounds obtained from the simplified model framework are applicable only in certain parameter space of Case C as we will show below. In general, we will find that the simplified model cannot reproduce the results derived from the renormalizable and gauge-invariant Higgs portal DM models. Thus we conclude that simplified models should be used for the DM search at colliders with great caution, keeping in mind its limited success.

This paper is organized as follows: In Section II, we first introduce the Lagrangian describing the renormalizable and gauge-invariant SFDM model and compare it with the Lagrangian of the simplified model in Eq. (1.1). Then, various constraints on the SFDM model from the measurements of the 125 GeV Higgs boson as well as direct searches for an extra Higgs boson are discussed. In Section III, we discuss the impact of the 125 GeV h_1 on the total cross section as well as the differential cross section for $pp \rightarrow t\bar{t}\chi\bar{\chi}$ in four different cases. For Case A and Case B, this process is dominated by the mediation of h_1 with $h_2 \sim S$ being irrelevant in most regions of m_{h_2} . For Case C and Case D, while the cross section in the SFDM model can be larger or smaller than that in the simplified model, the $p_T^{\chi\bar{\chi}}$ distribution in the SFDM model is always softer, resulting in a smaller cut efficiency. In Section IV, we show the LHC bounds in the SFDM model and compare them with those in the simplified model. In Section V, we summarize our results.

II. SFDM MODEL

The renormalizable and gauge-invariant Lagrangian that describes the SM extended with a gauge singlet fermion $\chi \sim (1, 1, 0)^1$ and a real singlet scalar S , i.e., the SFDM model, is [22, 23, 26, 27, 31, 32]

$$\mathcal{L} = -(y_u \bar{Q}_L \tilde{H} u_R + y_d \bar{Q}_L H d_R) + \bar{\chi}(i\not{\partial} - m_\chi - g_\chi S)\chi + \frac{1}{2}\partial_\mu S \partial^\mu S - V(H, S), \quad (2.1)$$

where y_u and y_d are the SM Yukawa couplings to the up- and down-type quarks, respectively, with suppressed generation indices. The interaction $\bar{Q}_L \tilde{H} \chi_R$ is forbidden by the $U(1)_Y$ symmetry while the interaction $\bar{L}_L \tilde{H} \chi_R$ can be discarded by a Z_2 symmetry under which only χ is odd, i.e., $\chi \rightarrow -\chi$ [27] or by global $U(1)$ symmetry [33].

The scalar potential of the SFDM is given by [27, 34]

$$\begin{aligned} V(H, S) = & -\mu_H^2 H^\dagger H + \lambda_H (H^\dagger H)^2 + \lambda_{HS} S^2 H^\dagger H + \mu_1 S H^\dagger H \\ & + \mu_0^3 S + \frac{1}{2} m_0^2 S^2 + \frac{\mu_2 S^3}{3!} + \frac{\lambda_S S^4}{4!}. \end{aligned} \quad (2.2)$$

The fields h and s are introduced after electroweak symmetric breaking as

$$H \rightarrow \begin{pmatrix} 0 \\ \frac{h + v_H}{\sqrt{2}} \end{pmatrix}, \quad S \rightarrow s + v_S, \quad (2.3)$$

where v_H and v_S are the vacuum expectation values of H and S , respectively. The mass matrix of the scalar fields is

$$\mathcal{M}^2 = \begin{pmatrix} 3\lambda_H v_H^2 - \mu_H^2 + v_S^2 \lambda_{HS} + v_S \mu_1 & v_H (2v_S \lambda_{HS} + \mu_1) \\ v_H (2v_S \lambda_{HS} + \mu_1) & \frac{1}{2} (2m_0^2 + 2v_H^2 \lambda_{HS} + v_S^2 \lambda_S + 2v_S \mu_2) \end{pmatrix}, \quad (2.4)$$

so that the mass eigenstates h_1 and h_2 can be defined as

$$\begin{pmatrix} h_1 \\ h_2 \end{pmatrix} = \begin{pmatrix} \cos \theta & -\sin \theta \\ \sin \theta & \cos \theta \end{pmatrix} \begin{pmatrix} h \\ s \end{pmatrix} \quad (2.5)$$

with

$$\tan(2\theta) = \frac{4v_H (2\lambda_{HS} v_S + \mu_1)}{v_H^2 (2\lambda_{HS} - 6\lambda_H) + 2\mu_H^2 - 2\lambda_{HS} v_S^2 + 2m_0^2 + \lambda_S v_S^2 - 2\mu_1 v_S + 2\mu_2 v_S}. \quad (2.6)$$

¹ For χ in a nontrivial representation of the SM gauge groups, see Refs. [29, 30]

It is well known [30, 35–38] that, for the most general Lagrangian that describes a real singlet scalar extension of the SM, there is a *shift symmetry* $S \rightarrow S + \Delta_S$, which holds in the SFDM model even though χ is introduced [32]. Thus we can freely choose $\langle S \rangle = 0$ without loss of generality in this paper.

The minimal conditions

$$\left. \frac{\partial V}{\partial H} \right|_{\langle H \rangle = v_H/\sqrt{2}} = 0, \quad (2.7)$$

$$\left. \frac{\partial V}{\partial S} \right|_{\langle S \rangle = 0} = 0 \quad (2.8)$$

lead to

$$\mu_H^2 = \lambda_H v_H^2, \quad (2.9)$$

$$\mu_0^3 = -\mu_1 v_H^2/2. \quad (2.10)$$

In the basis of $\langle S \rangle = 0$, the mixing between S and H comes solely from the term $\mu_1 S H^\dagger H$ in Eq. (2.2), and the mass matrix is simplified to

$$\mathcal{M}^2 = \begin{pmatrix} 2v_H^2 \lambda_H & v_H \mu_1 \\ v_H \mu_1 & v_H^2 \lambda_{HS} + m_0^2 \end{pmatrix}. \quad (2.11)$$

Introducing the variable [35]

$$y \equiv \frac{-2\mu_{hs}^2}{\mu_h^2 - \mu_s^2} \quad (2.12)$$

with

$$\mu_h^2 = 2v_H^2 \lambda_H, \quad \mu_s^2 = v_H^2 \lambda_{HS} + m_0^2, \quad \mu_{hs}^2 = v_H \mu_1, \quad (2.13)$$

the eigenvalues of the mass matrix can be expressed as

$$m_{h_{1,2}}^2 = \frac{\mu_h^2 + \mu_s^2}{2} \pm \frac{\mu_h^2 - \mu_s^2}{2} \sqrt{1 + y^2}, \quad (2.14)$$

where the sign $+$ ($-$) corresponds to m_{h_1} (m_{h_2}), and the mixing angle

$$\tan \theta = \frac{y}{1 + \sqrt{1 + y^2}}, \quad \tan(2\theta) = y. \quad (2.15)$$

It is noted that h_1 is SM-like while h_2 is singlet-like for $\theta \in [-\pi/4, \pi/4]$.

In terms of mass eigenstates, the interaction Lagrangian of interest can be written as

$$\begin{aligned} \mathcal{L}_{\text{int}} = & -(h_1 \cos \theta + h_2 \sin \theta) \left(\sum_f \frac{m_f}{v_H} \bar{f} f - \frac{2m_W^2}{v_H} W_\mu^+ W^{-\mu} - \frac{m_Z^2}{v_H} Z_\mu Z^\mu \right) \\ & + g_\chi (h_1 \sin \theta - h_2 \cos \theta) \bar{\chi} \chi . \end{aligned} \quad (2.16)$$

The couplings of h_1 and h_2 to the SM fermion pair ($f\bar{f}$) or weak gauge boson pair (VV) with $V = W$ or Z are given by

$$g_{h_1 xx} = c_\theta g_{hxx}^{\text{SM}}, \quad g_{h_2 xx} = s_\theta g_{hxx}^{\text{SM}}, \quad (2.17)$$

where $xx = f\bar{f}, VV$, g_{hxx}^{SM} is the corresponding SM coupling, $c_\theta \equiv \cos \theta$ and $s_\theta \equiv \sin \theta$. The couplings of h_1 and h_2 to the DM pair $\chi\bar{\chi}$ are

$$g_{h_1 \chi \bar{\chi}} = s_\theta g_\chi, \quad g_{h_2 \chi \bar{\chi}} = c_\theta g_\chi. \quad (2.18)$$

Now we can ask if the usual simplified model, Eq. (1.1), can be derived from the renormalizable and gauge-invariant model Lagrangian, Eq. (2.16). For the phenomenology at pp colliders, there are two relevant energy scales in addition to the mass scales (m_{h_1}, m_{h_2}, m_χ , etc.) in the Lagrangian: total center of mass energy (\sqrt{s}) and the center of mass energy at which the reaction actually occurs ($\sqrt{\hat{s}} \equiv x_1 x_2 s$) with $0 \leq x_1, x_2 \leq 1$ being energy fractions of partons inside the protons. $\sqrt{\hat{s}}$ is relevant since it is nothing but the characteristic scale of the hard scattering at parton levels, whereas \sqrt{s} is important since it is highest energy scale provided by the pp colliders.

Above all, let us notice that the model Lagrangian considered in Ref. [10] can be obtained by simply removing by hand (or integrating out) the h_1 field in Eq. (2.16). However it is clear that this procedure is justified only if all the quantities \sqrt{s} , $\sqrt{\hat{s}}$, and m_{h_2} are (much) smaller than $m_{h_1} = 125$ GeV or $\sqrt{\hat{s}}$ is resonantly enhanced at m_{h_2} . Otherwise, we cannot ignore (or integrate out) h_1 in the model Lagrangian. One has to include the effects of both h_1 and h_2 , since the interference between them could be important in certain cases [17, 26, 27, 39, 40]. There is no systematic way to derive the usual SFDM model, Eq. (1.1), as a proper effective field theory from Eq. (2.16), if $m_{h_2} > m_{h_1}$. In the following, we will show explicitly a number of examples where the role of h_1 is significant and the results are qualitatively different from those in Ref. [10].

Due to the mixing of s and h as in the SFDM model, the triple scalar couplings of $h_1 - h_2 - h_2$ and $h_2 - h_1 - h_1$ are also relevant, which are given by [31, 36–38, 41–43]

$$\lambda_{122} = 3\lambda_H v_H s_\theta^2 c_\theta - 2\lambda_{HS} v_H c_\theta (s_\theta^2 - c_\theta^2/2) - \frac{1}{2}\mu_1 s_\theta (s_\theta^2 - 2c_\theta^2) - \frac{1}{2}\mu_2 c_\theta^2 s_\theta, \quad (2.19)$$

$$\lambda_{211} = 3\lambda_H v_H c_\theta^2 s_\theta - 2\lambda_{HS} v_H s_\theta (c_\theta^2 - s_\theta^2/2) + \frac{1}{2}\mu_1 c_\theta (c_\theta^2 - 2s_\theta^2) + \frac{1}{2}\mu_2 s_\theta^2 c_\theta, \quad (2.20)$$

respectively.

In the SFDM model with $v_S = 0$, the free parameters were chosen to be m_{h_1} , m_{h_2} , θ , λ_{HS} , μ_2 , λ_S , v_H , m_χ and g_χ [32]. Identifying m_{h_1} and v_H as $m_{h_1} = 125$ GeV, $v_H = 246$ GeV, we however choose the following parameters for the convenience of collider phenomenology

$$m_{h_2}, \theta, \lambda_1, \lambda_2, m_\chi, g_\chi, \quad (2.21)$$

where λ_1 and λ_2 are normalized triple scalar couplings defined as

$$\lambda_1 \equiv \frac{\lambda_{122}}{\lambda_{\text{SM}}}, \quad \lambda_2 \equiv \frac{\lambda_{211}}{\lambda_{\text{SM}}}, \quad \text{with} \quad \lambda_{\text{SM}} = \frac{m_{h_1}^2}{2v_H}. \quad (2.22)$$

The production cross sections of h_1 and h_2 at the LHC can be expressed as

$$\sigma(pp \rightarrow h_1 + X) = c_\theta^2 \sigma^{\text{SM}}(pp \rightarrow h(m_{h_1}) + X), \quad (2.23)$$

$$\sigma(pp \rightarrow h_2 + X) = s_\theta^2 \sigma^{\text{SM}}(pp \rightarrow h(m_{h_2}) + X). \quad (2.24)$$

The total widths of h_1 and h_2 are²

$$\Gamma_{h_1} = c_\theta^2 \Gamma_h^{\text{SM}}(m_{h_1}) + \Gamma(h_1 \rightarrow h_2 h_2) + \Gamma(h_1 \rightarrow \chi \bar{\chi}), \quad (2.25)$$

$$\Gamma_{h_2} = s_\theta^2 \Gamma_h^{\text{SM}}(m_{h_2}) + \Gamma(h_2 \rightarrow h_1 h_1) + \Gamma(h_2 \rightarrow \chi \bar{\chi}), \quad (2.26)$$

where $\Gamma_h^{\text{SM}}(m_{h_1})$ and $\Gamma_h^{\text{SM}}(m_{h_2})$ correspond to the total decay width of the SM Higgs boson [44] with the mass being m_{h_1} and m_{h_2} , respectively. The decay widths of h_1 and h_2 into $\chi \bar{\chi}$ are

$$\Gamma(h_1 \rightarrow \chi \bar{\chi}) = \frac{s_\theta^2 g_\chi^2 m_{h_1}}{8\pi} (1 - 4m_\chi^2/m_{h_1}^2)^{3/2} \theta(m_{h_1} - 2m_\chi), \quad (2.27)$$

$$\Gamma(h_2 \rightarrow \chi \bar{\chi}) = \frac{c_\theta^2 g_\chi^2 m_{h_2}}{8\pi} (1 - 4m_\chi^2/m_{h_2}^2)^{3/2} \theta(m_{h_2} - 2m_\chi), \quad (2.28)$$

² We have neglected the widths of three-body decays since their contributions are usually subdominant [41].

where the Heaviside step function $\theta(x) = 1$ for $x > 0$ and $\theta(x) = 0$ for $x \leq 0$ and m_χ is the DM mass. The widths of h_1 and h_2 into $h_2 h_2$ and $h_1 h_1$ are [36–38, 42, 43]

$$\Gamma(h_2 \rightarrow h_1 h_1) = \frac{\lambda_2^2 \lambda_{\text{SM}}^2 \sqrt{1 - 4m_{h_1}^2/m_{h_2}^2}}{8\pi m_{h_2}} \theta(m_{h_2} - 2m_{h_1}), \quad (2.29)$$

$$\Gamma(h_1 \rightarrow h_2 h_2) = \frac{\lambda_1^2 \lambda_{\text{SM}}^2 \sqrt{1 - 4m_{h_2}^2/m_{h_1}^2}}{8\pi m_{h_1}} \theta(m_{h_1} - 2m_{h_2}), \quad (2.30)$$

respectively. It is clear that the above widths are not sensitive to the signs of λ_1 and λ_2 . Therefore we shall concentrate on the magnitudes of λ_1 and λ_2 in the collider study for the SFDM model.

Since h_2 may also decay into an extended dark sector other than $\chi\bar{\chi}$, similar to the simplified models [1–4] we can introduce the *minimal* total width of h_2 in the SFDM model [26, 27]:

$$\Gamma_{h_2}^{\text{min}} = \Gamma_{h_2} \text{ with } \Gamma(h_2 \rightarrow h_1 h_1) = 0. \quad (2.31)$$

It should be emphasized that the minimal total width of h_2 in the SFDM model also includes the partial decay width into WW^* and ZZ^* , without which as in the simplified model the cancellation [45] between diagrams with $h_2 WW$ and $h_2 t\bar{t}$ interactions in DM production in association with single top quark $pp \rightarrow tj\chi\bar{\chi}$ does not occur and the sensitivity in $pp \rightarrow tj\chi\bar{\chi}$ can be even comparable to that in $pp \rightarrow t\bar{t}\chi\bar{\chi}$ [13, 14].

The mixing angle θ is constrained by the Higgs signal strength measurements: $\sin^2 \theta \lesssim 0.12$ at 95% confidence level (C.L.) [34, 46, 47], while constraints from heavy Higgs boson direct searches [38, 48–50] and the electroweak precision observables [23, 34, 42, 43] are found to be weaker than the Higgs signal strength measurements.³ In this paper, we will fix $\sin \theta$ to be 0.2 conservatively.

The current 95% C.L. upper limits on the invisible decay branching ratio and the total width of the 125 GeV Higgs boson are 0.24 [46, 51, 52] and 0.13 GeV [53], respectively. In the left panel of Fig. 1, we show the constraints in the $g_\chi - m_\chi$ plane with $\sin \theta = 0.2$ and $\Gamma(h_1 \rightarrow h_2 h_2) = 0$, which indicates that the constraint from the invisible decay branching ratio of the 125 GeV Higgs boson is stronger than that from its total width. If $m_{h_1} > 2m_{h_2}$, the decay channel $h_1 \rightarrow h_2 h_2$ is kinematically allowed. In the right panel of Fig. 1, the

³ It is however found in Refs. [34, 42] that the constraint on θ from direct searches can be slightly stronger for the heavy Higgs boson mass below 450 GeV in the SM with a singlet scalar. But it is relaxed in the SFDM model if $m_\chi < m_{h_2}/2$ so that $h_2 \rightarrow \chi\bar{\chi}$ is kinematically open.

constraints in the $g_\chi - \lambda_1$ plane from the invisible decay branching ratio and total width of h_1 and the branching ratio into the beyond SM (BSM) decays $\text{Br}_{h_1}^{\text{BSM}} < 0.34$ [47]⁴ with $\sin\theta = 0.2$, $m_\chi = 50$ GeV and $m_{h_2} = 54.3$ GeV are displayed. We will show in Section III that, such benchmark values of m_χ and m_{h_2} are appropriate for Case B.

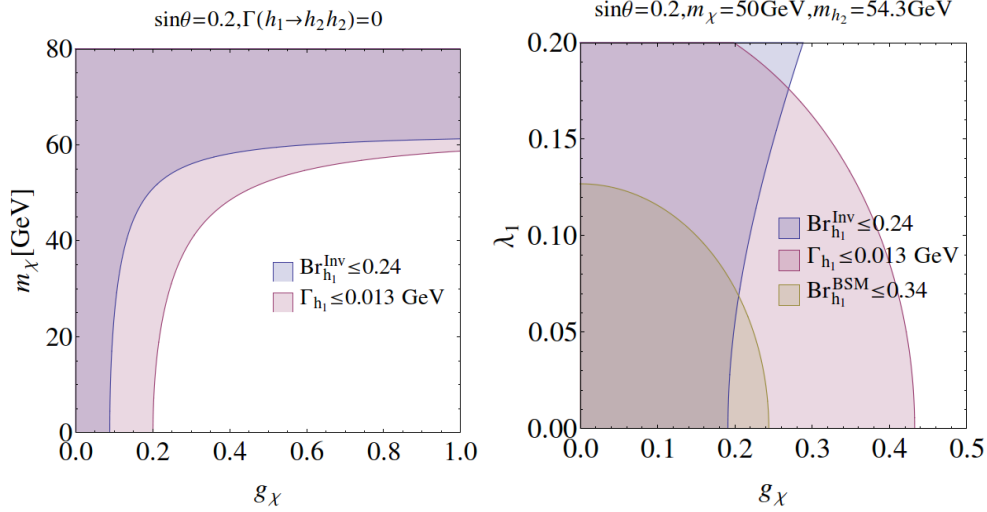


FIG. 1: The allowed regions by the invisible decay branching ratio (blue), total width (red) and BSM decay branching ratio (orange) of h_1 in the SFDM model with $\sin\theta = 0.2$. Left panel: $\Gamma(h_1 \rightarrow h_2 h_2) = 0$. Right panel: $m_\chi = 50$ GeV and $m_{h_2} = 54.3$ GeV.

On the other hand, searches for di-Higgs production play a key role in the determination of the triple scalar coupling λ_2 . The cross section of $pp \rightarrow h_1 h_1$ can be parameterized as⁵

$$\sigma(pp \rightarrow h_1 h_1) = \sigma^{\text{SM}}(pp \rightarrow h_2) \times s_\theta^2 \frac{\lambda_2^2 f(m_{h_2})}{s_\theta^2 + c_\theta^2 g_\chi^2 g(m_{h_2}) + \lambda_2^2 f(m_{h_2})}, \quad (2.32)$$

with

$$f(m_{h_2}) = \frac{\lambda_{\text{SM}}^2 \sqrt{1 - 4m_{h_1}^2/m_{h_2}^2}}{8\pi m_{h_2} \Gamma^{\text{SM}}(m_{h_2})}, \quad (2.33)$$

$$g(m_{h_2}) = \frac{m_{h_2} (1 - 4m_\chi^2/m_{h_2}^2)^{3/2}}{8\pi \Gamma^{\text{SM}}(m_{h_2})} \theta(m_{h_2} - 2m_\chi). \quad (2.34)$$

Figure 2 shows the di-Higgs production cross section in the SFDM model (assuming $\Gamma(h_2 \rightarrow \chi \bar{\chi}) = 0$ and $\sin\theta = 0.2$) alongside the combined upper limit at the 13 TeV

⁴ We find that light boson direct searches [54] can also directly constrain the triple scalar coupling λ_1 . But as found in Ref [55], the constraint from the light boson direct searches is much weaker than that from the BSM decay branching ratio.

⁵ In reality, the coupling of $h_1 - h_1 - h_1$ can contribute to the non-resonant production of $h_1 h_1$, which is neglected here.

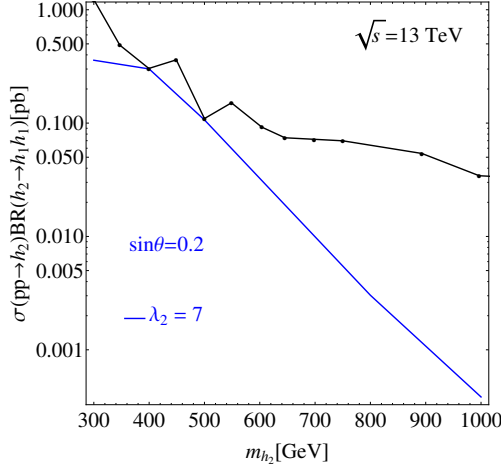


FIG. 2: Constraints on λ_2 from resonant di-Higgs searches at the 13 TeV LHC.

LHC [56], which implies that $\lambda_2 < 7$. On the other hand, the theoretical constraint on λ_2 can be found in Ref. [38], which is $\lambda_2 \lesssim 10$. For $\Gamma(h_2 \rightarrow \chi\bar{\chi}) \neq 0$, larger λ_2 could be allowed depending on the mass m_χ and also the coupling g_χ , which will not be studied in details in this paper.

In Fig. 3, the total width of h_2 for $\sin\theta = 0.2$, $m_\chi = 65$ GeV (for a larger m_χ , the total width is smaller) is displayed. We can find that for $g_\chi \lesssim 1$, the ratio Γ_{h_2}/m_{h_2} is below 10% and $\Gamma_{h_2}/m_{h_2} < 1$ can still be satisfied even with $g_\chi = 5$. To evaluate the impact of the decay $h_2 \rightarrow h_1 h_1$, we further show the branching ratio of $h_2 \rightarrow \chi\bar{\chi}$ for various parameter choices in Fig. 4. One can find that including $h_2 \rightarrow h_1 h_1$ can decrease $\text{Br}(h_2 \rightarrow \chi\bar{\chi})$ especially for smaller g_χ . However it does not affect much the behavior of interplay between h_1 and h_2 in the DM search in Section III, so we will keep $\lambda_2 = 0$ for simplicity hereafter.

In the SFDM model, the DM pair can annihilate into either SM gauge bosons/fermions through h_1/h_2 mediation or scalar bosons through t -channel/ s -channel process if it is kinematically allowed. The annihilation cross section of the former is proportional to g_χ^2 while that of the latter is proportional to g_χ^4 (g_χ^2) for t -channel (s -channel) annihilation. So a large g_χ is required to annihilate the DM effectively, which renders the DM direct detections quite stringent (except in the resonant region of the s -channel process $m_\chi \sim m_{h_{1,2}}/2$). The details of the DM thermal relic density and the spin-independent DM-nucleon scattering cross section for benchmark points in each case are provided in the Appendix. In order to guarantee that the DM has a relic density below the observation and keep consistent with the DM direct detections, the SFDM model should be generalized beyond the minimal setup of the

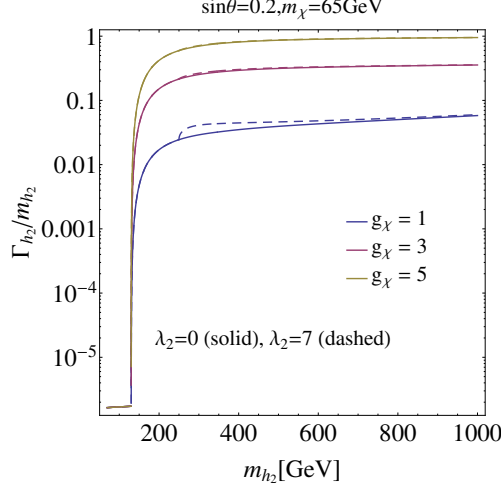


FIG. 3: The ratios Γ_{h_2}/m_{h_2} with respect to m_{h_2} for different g_χ values, where $\sin \theta = 0.2$, $m_\chi = 65$ GeV. For larger m_χ , the ratio is smaller. The ratios with (without) including $h_2 \rightarrow h_1 h_1$ partial width are denoted by solid (dashed) curves.

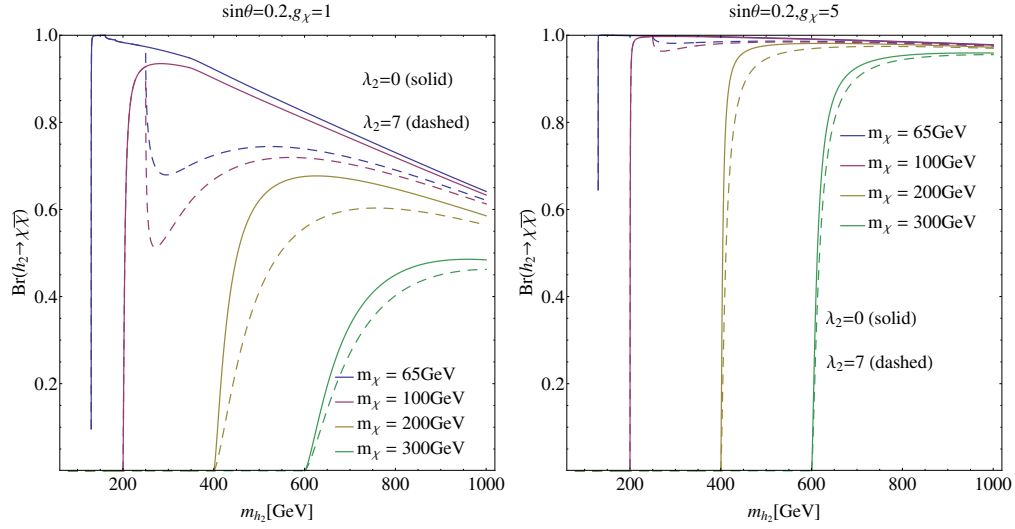


FIG. 4: Branching ratios of $h_2 \rightarrow \chi\bar{\chi}$ with varying m_χ , where Γ_{h_2} is defined in Eq. (2.26). Left: $g_\chi = 1$; right: $g_\chi = 5$. The branching ratios without (with) the decay $h_2 \rightarrow h_1 h_1$ are denoted by solid (dashed) curves.

Higgs portal SFDM model. New DM annihilation channels should be introduced, such as $\chi\bar{\chi} \rightarrow Z'Z'$ if DM is charged under a dark $U(1)$ gauge group [57–60], or coannihilation channels if there are more particles in the DM sector that have a mass close to the DM [61]. Then the dark matter direct detection constraints can be weakened or even completely evaded. Moreover, the particle χ discussed in the current paper may correspond to a heavier dark

state in the dark sector that can decay into the genuine DM candidate. Then, as long as the heavier dark state(s) does not leave any signal at the detector (due to a long lifetime or invisible decay), it will produce the same collider phenomenology as the SFDM model ⁶.

III. $t\bar{t} + \cancel{E}_T$ SIGNATURE

Now we are ready to study the impact of the 125 GeV Higgs boson h_1 in the DM search with $t\bar{t} + \cancel{E}_T$ signature. Previous studies in the mono-jet, VBF and mono-V signatures can be found in Refs. [26, 27]. The $t\bar{t} + \cancel{E}_T$ channel at the 8 TeV LHC was preformed in Ref. [26], and compared with the CMS results.

There are two mediators in $pp \rightarrow t\bar{t}\chi\bar{\chi}$ in the SFDM model, which are shown in Fig. 5. The total amplitude is then proportional to

$$\mathcal{A} \propto g_\chi \sin(2\theta) \left(\frac{1}{\hat{s} - m_{h_1}^2 + im_{h_1}\Gamma_{h_1}} - \frac{1}{\hat{s} - m_{h_2}^2 + im_{h_2}\Gamma_{h_2}} \right), \quad (3.1)$$

where $\hat{s} \equiv m_{\chi\bar{\chi}}^2$ with $m_{\chi\chi}$ being the invariant mass of the DM pair $\chi\bar{\chi}$. Therefore the diagrams with h_1 and the ones with h_2 interfere destructively for $\sqrt{\hat{s}} > m_{h_1}, m_{h_2}$ or $\sqrt{\hat{s}} < m_{h_1}, m_{h_2}$ and constructively for $m_{h_1} < \sqrt{\hat{s}} < m_{h_2}$ or $m_{h_2} < \sqrt{\hat{s}} < m_{h_1}$. Note that in the simplified model (see Eq. (1.1)) only h_2 in Fig. 5 is included, in contrast with the renormalizable and gauge-invariant SFDM model.

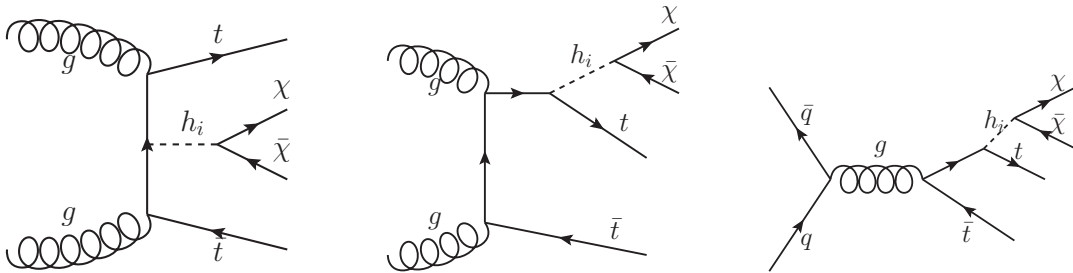


FIG. 5: Feynman diagrams of $pp \rightarrow t\bar{t}\chi\bar{\chi}$ in the SFDM model with mediators $h_i = h_1, h_2$.

Depending on the relations of m_{h_1} , m_{h_2} and m_χ , the process $pp \rightarrow t\bar{t}\chi\bar{\chi}$ in the SFDM model can be categorized into four cases, namely,

- Case A: $m_{h_1}, m_{h_2} > 2m_\chi$,

⁶ Work in progress.

- Case B: $m_{h_1} > 2m_\chi$ and $m_{h_2} < 2m_\chi$,
- Case C: $m_{h_1} < 2m_\chi$ and $m_{h_2} > 2m_\chi$, and
- Case D: $m_{h_1}, m_{h_2} < 2m_\chi$.

In the following, we will denote the cross section of diagrams with each scalar mediator (h_1/h_2) as σ_{h_1} and σ_{h_2} , while the total cross section that includes the interference effect between diagrams with different mediators is denoted as $\sigma_{h_1+h_2}$.

For Case A, both h_1 and h_2 can be on-shell in DM production, so that the cross sections can be described as

$$\sigma_{h_1} = c_\theta^2 \sigma^{\text{prod}}(m_{h_1}) \text{Br}(h_1 \rightarrow \chi\bar{\chi}), \quad (3.2)$$

$$\sigma_{h_2} = s_\theta^2 \sigma^{\text{prod}}(m_{h_2}) \text{Br}(h_2 \rightarrow \chi\bar{\chi}) \quad (3.3)$$

with the narrow width approximation (NWA), where $\sigma^{\text{prod}}(m_{h_i})$ denotes the cross section of $pp \rightarrow t\bar{t}h_i$ for on-shell h_i , $i = 1, 2$ with SM couplings. In this case, the interference effect is small unless $m_{h_2} \simeq m_{h_1}$; thus, the cross section with two mediators is approximately equal to the sum of the cross sections with one mediator:

$$\sigma_{h_1+h_2} \simeq \sigma_{h_1} + \sigma_{h_2}. \quad (3.4)$$

In the left panel of Fig. 6, we show the leading-order (LO) cross section of $pp \rightarrow t\bar{t}\chi\bar{\chi}$ at the 13 TeV LHC for Case A with $g_\chi = 0.08$, $m_\chi = 1$ GeV, $\Gamma_{h_2} = \Gamma_{h_2}^{\text{min}}$ and $m_{h_2} \gtrsim 65$ GeV satisfying the constraint from the invisible decay branching ratio of h_1 . We find that the h_2 provides a larger cross section than the h_1 when $m_{h_2} \lesssim 70$ GeV. With increasing m_{h_2} , the contribution from h_2 decreases dramatically and becomes negligible for $m_{h_2} \gtrsim 300$ GeV, in which scenario the process $pp \rightarrow t\bar{t}\chi\bar{\chi}$ is effectively described by a single mediator h_1 . Note that here we assume $\Gamma_{h_2} = \Gamma_{h_2}^{\text{min}}$. If we consider the decay of h_2 into $h_1 h_1$, which is possible if $m_{h_2} > 2m_{h_1}$, the branching ratio of $h_2 \rightarrow \chi\bar{\chi}$ will be suppressed. On the other hand, h_1 can also decay into $h_2 h_2$ if $m_{h_2} < m_{h_1}/2$ so that the branching ratio of $h_1 \rightarrow \chi\bar{\chi}$ is suppressed. This fact will bring the m_{h_2} dependence to the cross section of σ_{h_1} , which is not shown in the Fig. 6.

For Case B, only h_1 can be on-shell so that the contribution of h_1 is dominant and

$$\sigma_{h_1+h_2} \simeq \sigma_{h_1}. \quad (3.5)$$

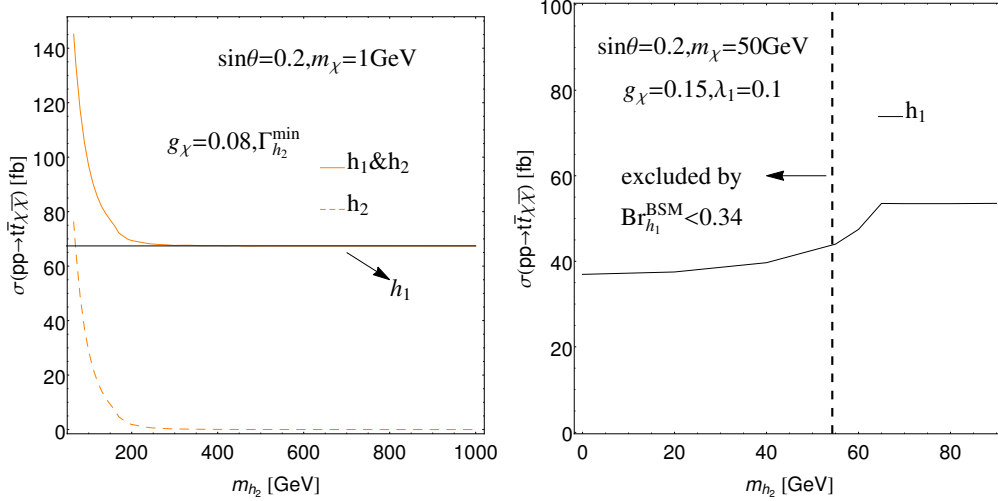


FIG. 6: Cross sections of $pp \rightarrow t\bar{t}\chi\bar{\chi}$ at the 13 TeV LHC for Case A (left panel) with $g_\chi = 0.08$, $m_\chi = 1$ GeV and $\Gamma_{h_2} = \Gamma_{h_2}^{\min}$ and for Case B (right panel) with $g_\chi = 0.15$, $\lambda_1 = 0.1$ and $m_\chi = 50$ GeV, where $m_{h_2} \lesssim 54.3$ GeV is excluded by the BSM decay branching ratio of h_1 .

In the right panel of Fig. 6, we show the cross section of $pp \rightarrow t\bar{t}\chi\bar{\chi}$ at the 13 TeV LHC for Case B with $g_\chi = 0.15$, $\lambda_1 = 0.1$, and $m_\chi = 50$ GeV. Similar to Case A, the cross section σ_{h_1} depends on m_{h_2} in the region of $m_{h_2} < m_{h_1}/2$. Considering the constraint from the BSM decay branching ratio of h_1 , $\text{Br}_{h_1}^{\text{BSM}} < 0.34$ [47], h_2 with $m_{h_2} \lesssim 54.3$ GeV is excluded for our parameter choice.

For Case C, only h_2 can be on-shell. If $\Gamma_{h_2}/m_{h_2} \ll 1$, which implies that the NWA can be applied, one obtains

$$\sigma_{h_1} \propto s_\theta^2 c_\theta^2 g_\chi^2, \quad (3.6)$$

$$\sigma_{h_2} = s_\theta^2 \sigma^{\text{prod}}(m_{h_2}) \text{Br}(h_2 \rightarrow \chi\bar{\chi}). \quad (3.7)$$

If $\Gamma_{h_2} = \Gamma_{h_2}^{\min}$, as shown in Fig. 4 the decay branching ratio $\text{Br}(h_2 \rightarrow \chi\bar{\chi})$ is relatively large for $g_\chi \sim 1$, which leads to $\sigma_{h_2} \gg \sigma_{h_1}$, so that the simplified model with single mediator h_2 can describes the SFDM model approximately. However, there are key differences between this case and Case B. Firstly, confronted with the measurements of the Higgs invisible decay branching ratio the coupling g_χ is severely constrained for Case B, while there is no such constraint on g_χ for Case C due to $m_{h_1} < 2m_\chi$. Thus the cross section with off-shell h_1 can be significantly enhanced for a large $g_\chi \sim 5$ [2, 10] as in Eq. (3.6). Secondly, unlike h_1

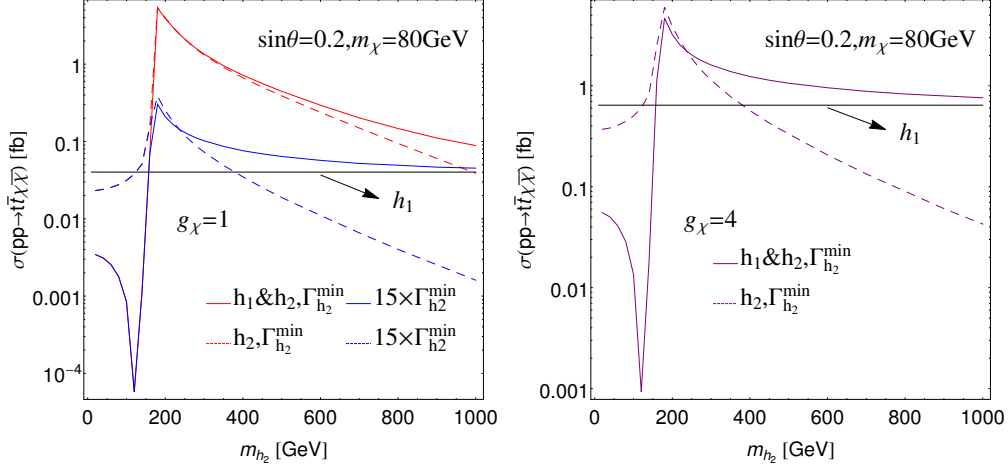


FIG. 7: Cross sections of $pp \rightarrow t\bar{t}\chi\bar{\chi}$ at the 13 TeV LHC for Case C and Case D. Left panel: $g_\chi = 1$, $m_\chi = 80$ GeV and $\Gamma_{h_2} = \Gamma_{h_2}^{\min}, 15 \times \Gamma_{h_2}^{\min}$; right panel: $g_\chi = 4$, $m_\chi = 80$ GeV and $\Gamma_{h_2} = \Gamma_{h_2}^{\min}$.

there is no direct experimental constraint on Γ_{h_2} . So if there exist other decay channels of h_2 , for example h_2 decays into extra dark sector particles [60], the total width of h_2 can be significantly enhanced as compared to $\Gamma_{h_2}^{\min}$. Consequently, the branching ratio of h_2 into $\chi\bar{\chi}$ is possibly small. Thus although h_1 is off-shell in DM production for Case C, its contribution should be taken into account, which however has not been paid much attention to. It should be noted that the wide width of h_2 may make the NWA in Eq. (3.7) invalid.

For Case D, both h_1 and h_2 are off-shell, so that the cross sections

$$\sigma_{h_1} \propto s_\theta^2 c_\theta^2 g_\chi^2, \quad (3.8)$$

$$\sigma_{h_2} \propto s_\theta^2 c_\theta^2 g_\chi^2 \quad (3.9)$$

are small but the interference effect between diagrams with different mediators in Fig. 5 is significant and always destructive, as can be seen from Eq. (3.1).

To consider the wide width effects, we assume that the total width of h_2 is rescaled by a factor of 15 irrespective of its mass, i.e., $\Gamma_{h_2} = 15 \times \Gamma_{h_2}^{\min}$, which satisfies $\Gamma_{h_2}/m_{h_2} < 1$ as shown in Fig. 3. Then, the cross section of $pp \rightarrow t\bar{t}\chi\bar{\chi}$ with h_2 mediation is reduced by a factor of about 15. On the other hand, a larger coupling g_χ can also increase the h_2 decay width as well as enhance the σ_{h_1} . To compare with the simplified model study in Refs. [2, 10], we choose $g_\chi = 4$. In Fig. 7, we show the cross sections of $pp \rightarrow t\bar{t}\chi\bar{\chi}$ at the 13 TeV LHC for Case C and Case D with $g_\chi = 1$, $m_\chi = 80$ GeV, and $\Gamma_{h_2} = \Gamma_{h_2}^{\min}(15 \times \Gamma_{h_2}^{\min})$ in

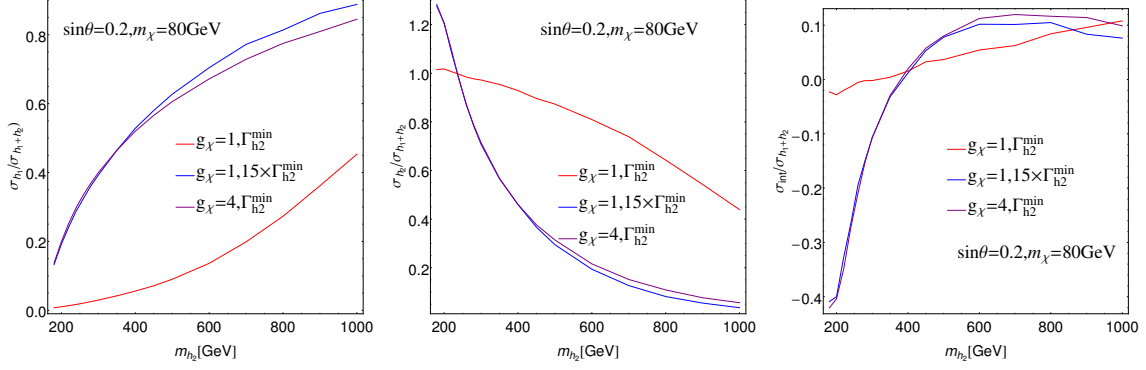


FIG. 8: The relative contributions of mediators h_1 , h_2 and their interference to the total cross section for Case C.

the left panel and $g_\chi = 4$, $m_\chi = 80$ GeV, and $\Gamma_{h_2} = \Gamma_{h_2}^{\min}$ in the right panel.

We find that $\sigma_{h_1+h_2} < \sigma_{h_1} + \sigma_{h_2}$ in the region of $m_{h_2} \lesssim 2m_\chi$ (Case D) irrespective of g_χ and Γ_{h_2} . This is due to the destructive interference between diagrams with h_1 and h_2 in case D. The destructive interference effect is most significant at $m_{h_2} \simeq m_{h_1}$.

For $m_{h_2} \gtrsim 2m_\chi$ (Case C), the contributions of h_1 and h_2 depend on the coupling g_χ and the total width of h_2 as we discussed above. For illustration, in Fig. 8 we show the relative contributions of mediator h_1 , mediator h_2 and their interference contributions to the total cross sections denoted as $\sigma_{h_1}/\sigma_{h_1+h_2}$, $\sigma_{h_2}/\sigma_{h_1+h_2}$ and $\sigma_{\text{int}}/\sigma_{h_1+h_2}$. For $g_\chi = 1$ and $\Gamma_{h_2} = \Gamma_{h_2}^{\min}$, it is observed that $\sigma_{h_2}/\sigma_{h_1+h_2}$ is approximately equal to 1 for $m_{h_2} \simeq 200$ GeV and decreases with larger m_{h_2} . On the other hand, both $\sigma_{h_1}/\sigma_{h_1+h_2}$ and $\sigma_{\text{int}}/\sigma_{h_1+h_2}$ become more important with the increase of m_{h_2} . For example, $\sigma_{h_1} : \sigma_{h_2} : \sigma_{\text{int}} = 0.087 : 0.87 : 0.037$ for $m_{h_2} = 500$ GeV and $\sigma_{h_1} : \sigma_{h_2} : \sigma_{\text{int}} = 0.45 : 0.45 : 0.1$ for $m_{h_2} = 1000$ GeV. The interference effect is destructive in the region of $2m_\chi \lesssim m_{h_2} \lesssim 380$ GeV and constructive for $m_{h_2} \gtrsim 380$ GeV. The impact of h_1 becomes even more significant for $\Gamma_{h_2} = 15 \times \Gamma_{h_2}^{\min}$ or $g_\chi = 4$.

Until now we have only discussed the impact of the mediator h_1 on the total cross section, in which the $m_{\chi\bar{\chi}}$ dependence has been integrated out. From Eq. (3.1), we see that the interference effect depends on the interplay of $m_{\chi\bar{\chi}}^2 - m_{h_1}^2$ with $m_{\chi\bar{\chi}}^2 - m_{h_2}^2$. For example, the interference is constructive (destructive) for $m_{\chi\bar{\chi}}^2 - m_{h_2}^2 < (>) 0$ for Case C. To study the impact of h_1 on the differential cross section, the invariant mass distributions of $\chi\bar{\chi}$ are displayed with $m_\chi = 80$ GeV, $m_{h_2} = 200, 300, 500$ GeV, $g_\chi = 1$ and $\Gamma_{h_2} = 15 \times \Gamma_{h_2}^{\min}$ (similar for $g_\chi = 4$ and $\Gamma_{h_2} = \Gamma_{h_2}^{\min}$) in Fig. 9. Unlike the distribution with on-shell h_2 (blue dashed

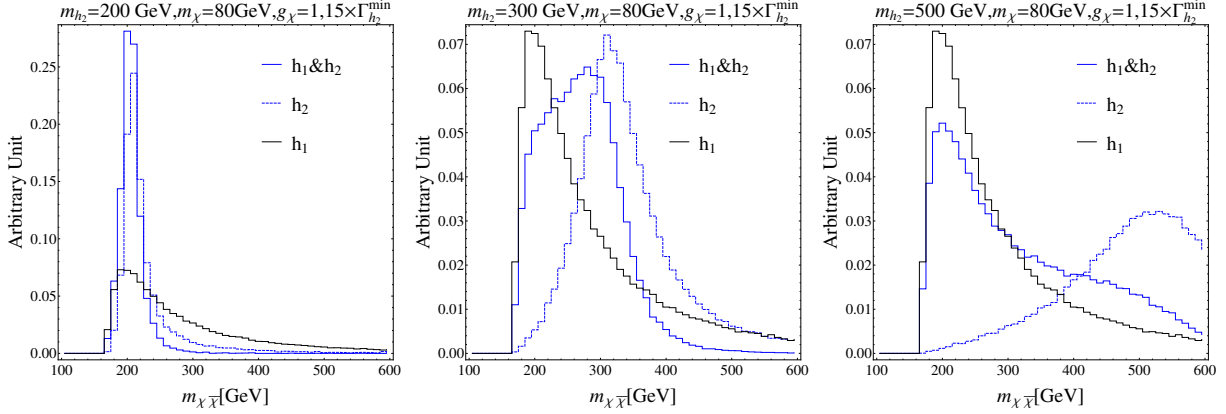


FIG. 9: The distributions of $m_{\chi\bar{\chi}}$ with mediators h_1 and h_2 for Case C with $m_{\chi} = 80$ GeV, $m_{h_2} = 200, 300, 500$ GeV, $g_{\chi} = 1$ and $\Gamma_{h_2} = 15 \times \Gamma_{h_2}^{\min}$.

curve), which centers around $m_{\chi\bar{\chi}} \sim m_{h_2}$, the distribution with off-shell h_1 (black curve) decreases rapidly with increasing $m_{\chi\bar{\chi}}$. As a result, the distribution with two mediators tends to be softer than that in the simplified model with h_2 . Moreover, the distribution with two mediators is asymmetric around m_{h_2} : More events fall into region of $m_{\chi\bar{\chi}}^2 - m_{h_1}^2 > 0$ for $m_{h_2} = 200$ and 300 GeV, while fewer are in the region of $m_{\chi\bar{\chi}}^2 - m_{h_1}^2 > 0$ for $m_{h_2} = 500$ GeV. After integrating over $m_{\chi\bar{\chi}}$, the interference effect in the total cross section is destructive for $m_{h_2} = 200$ and 300 GeV and constructive for $m_{h_2} = 500$ GeV as shown in the right panel of Fig. 8.

Experimentally, the invariant mass of $\chi\bar{\chi}$ cannot be reconstructed directly. However, its feature can be reflected in the distribution of the transverse momentum of $\chi\bar{\chi}$ (missing transverse momentum), i.e., $p_T^{\chi\bar{\chi}}$. In Fig. 10 we show the parton-level distributions of $p_T^{\chi\bar{\chi}}$ for Case C with $m_{\chi} = 80$ GeV, $m_{h_2} = 200, 300, 500$ GeV, $g_{\chi} = 1$ and $\Gamma_{h_2} = 15 \times \Gamma_{h_2}^{\min}$ (similar for $g_{\chi} = 4$ and $\Gamma_{h_2} = \Gamma_{h_2}^{\min}$). One can obtain that $p_T^{\chi\bar{\chi}}$ distribution in the SFDM model with two mediators is always softer than that in the simplified model with h_2 , the effect of which on the cut efficiency of a concrete experimental search will be discussed in Section IV.

IV. IMPACT ON THE UPPER LIMITS

Having observed the distinct difference between the total cross sections and differential distributions of $pp \rightarrow t\bar{t}\chi\bar{\chi}$ with two mediators and with one mediator, we will investigate the impact of the Higgs boson h_1 on the 95% C.L. upper limits of searches for DM produced

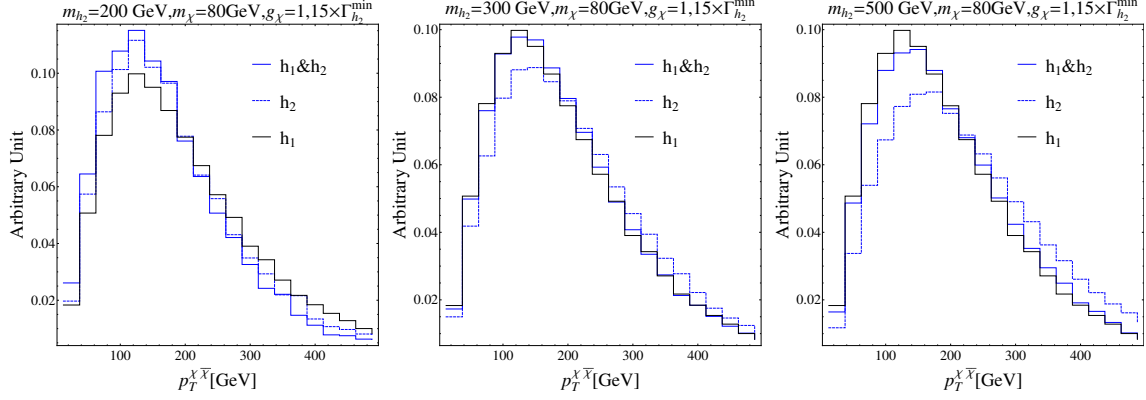


FIG. 10: The parton-level distributions of $p_T^{\chi\bar{\chi}}$ for Case C with $m_\chi = 80$ GeV, $m_{h_2} = 200, 300, 500$ GeV, $g_\chi = 1$ and $\Gamma_{h_2} = 15 \times \Gamma_{h_2}^{\min}$.

with top quark pair at the 13 TeV LHC, which have been performed by the CMS and ATLAS Collaborations in the hadronic, semileptonic and dileptonic channels [19, 21, 62, 63]. Similar to Ref. [13], we closely follow the CMS analyses [21, 62, 63] and concentrate on the hadronic and semileptonic channels since the dileptonic are typically less sensitive in these analyses. On the other hand, although recent search using events with 35.9 fb^{-1} [21] has improved the upper limit significantly as compared to that with 2.2 fb^{-1} [62, 63], the background event numbers in signal regions are not provided [21]. Therefore we take the strategy that we first recast the results with 2.2 fb^{-1} and then project them to the integrated luminosity of 36 fb^{-1} with the assumption that the signal and background uncertainties scale as the integrated luminosity and the square root of the integrated luminosity, respectively. Another reason for projection is that a multivariate discriminant “resolved top tagger” was used in the analysis [21] without giving any details for recasting.⁷ In our analysis, we only consider the inclusive hadronic channel without using “resolved top tagger” similar to Ref. [13].

We generate the signal process $pp \rightarrow t\bar{t}\chi\bar{\chi}$ using **MG5_aMC@NLO** v2.4.3 [64] at leading order in the 5-flavor scheme. The parton-level events are then passed to **Pythia6** [65] for parton showering and hadronization. The detector effects are included by using **Delphes3** v3.3.3 [66] and **Fastjet** [67] packages, in which jets are clustered using the anti- k_t algorithm with $R = 0.4$. The b -tagging efficiency is 0.6, while the c quark and light quark faking rates

⁷ Due to these limitations, it is not possible to compare our upper limits with 36 fb^{-1} to Ref. [21] directly.

However we have validated our result by simulating the signal process in the simplified model with $g_\chi = g_q = 1$ and $(m_\chi, m_\phi) = (1 \text{ GeV}, 100 \text{ GeV}), (1 \text{ GeV}, 200 \text{ GeV})$ and $(50 \text{ GeV}, 300 \text{ GeV})$. The discrepancies between our results and Refs. [13, 62, 63] are 13% and 23% in the inclusive hadronic and semileptonic channels, respectively, which indicates that our recast is reasonable.

are 0.07 and 0.01, respectively [13].

Having imposed the selection cuts [62, 63], the number of signal events with integrated luminosity \mathcal{L} is then

$$\mathcal{N}_{\text{signal}} = \sigma_{\text{before cut}} \times \epsilon \times \mathcal{L}, \quad (4.1)$$

where $\sigma_{\text{before cut}}$ denotes the cross section of $pp \rightarrow t\bar{t}\chi\bar{\chi}$ without any cut and ϵ denotes the cut efficiency in the hadronic or semileptonic channel.

The LHC search sensitivity to our models can be measured by the signal strength $\mu = \sigma/\sigma_{\text{th}}$, where σ denotes the observed production cross section of $pp \rightarrow t\bar{t}\chi\bar{\chi}$ at the 13 TeV LHC and σ_{th} is the theoretical signal cross section. The 95% C.L. upper limit on μ is investigated using the CLs method [68–70], with inputs of production cross section and cut efficiencies of a concrete model from our simulation as well as the number of background events and their uncertainties provided in the experimental papers [62, 63].

Then we will investigate the impact of the mediator h_1 on the upper limits μ in the SFDM model. From Eq. (4.1), we know that the number of signal events after selections depend on the total cross section of $pp \rightarrow t\bar{t}\chi\bar{\chi}$ as well as the cut efficiency. As having been discussed in Section III, for Case A and Case B, the signal production is dominated by the process with mediator h_1 . So adding h_1 will change both the production rate and the final state kinematics (i.e., cut efficiency) significantly. On the other hand, for Case C and Case D, both h_1 and h_2 have an impact on the signal production cross section and cut efficiency.

In Fig. 11, we show the 95% C.L. upper limits on μ in the inclusive hadronic (jets) and semileptonic ($\ell + \text{jets}$) channels [62, 63] in the SFDM model with two mediators as well as one mediator h_2 (identified as the simplified model) with the integrated luminosity of 36 fb^{-1} for Case A and Case B. In the left panel, we find that, although the couplings of the mediator(s) to the SM quarks and DM are small for Case A, the 95% C.L. upper limit on μ in the SFDM model can reach $\mu < 10$ and is nearly independent of m_{h_2} , while the upper limit in the simplified model is much weaker especially for a larger m_{h_2} . In the middle and right panels, we display the upper limits of the SFDM model for three benchmark values of g_χ and λ_1 for Case B. The measurements from the SM Higgs BSM decay branching ratio ($\text{Br}_{h_1}^{\text{BSM}} < 0.34$ [47]) can also constrain the parameter space for $m_{h_2} < m_{h_1}/2$ denoted as thick green curves. For smaller λ_2 , a more severe bound on μ can be obtained. The upper limit is sensitive to m_{h_2} only if $m_{h_2} < m_{h_1}/2$. Roughly speaking, the upper limit with the

integrated luminosity of 36 fb^{-1} is below 50 with these three benchmark values for Case B.

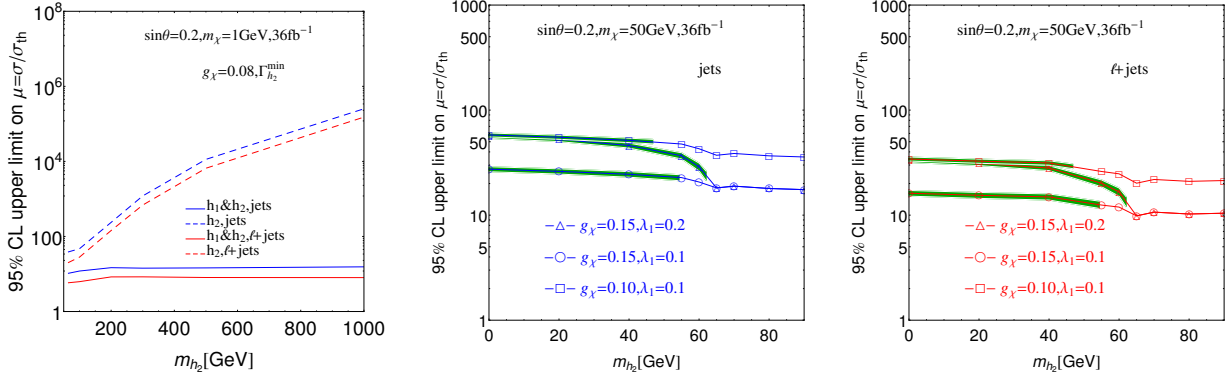


FIG. 11: The 95% C.L. upper limits on μ in the inclusive hadronic (jets) and semileptonic ($\ell + \text{jets}$) channels [62, 63]. Left panel: The upper limits for Case A in the SFDM model (solid curves) and in the simplified model (dashed curves). Middle and right panels: The upper limits on μ for Case B in the SFDM model for three benchmark values of g_χ and λ_1 . Parameter space of m_{h_2} denoted as thick green curves is excluded by the measurements of Higgs BSM decay branching ratio.

For Case C and Case D, both h_1 and h_2 play important roles in $pp \rightarrow t\bar{t}\chi\bar{\chi}$ in the SFDM model. Figure 12 shows the cut efficiencies for Case C and Case D in the inclusive hadronic and semileptonic channels in the SFDM model with two mediators as well as one mediator h_2 . Since the $p_T^{\chi\bar{\chi}}$ distribution in the SFDM model is softer than that in the simplified model (see Fig. 10), a lower cut efficiency is achieved in the former scenario. On the other hand, in both scenarios the cut efficiencies are lowest when m_{h_2} is around 180 GeV. This is because the DM pairs $\chi\bar{\chi}$ are mostly produced through the on-shell h_2 mediation while events with $m_{\chi\bar{\chi}} > m_{h_2}$ are suppressed by the destructive interference between h_1 and h_2 in the SFDM model and the h_2 propagator in the simplified model. As a result, the $p_T^{\chi\bar{\chi}}$ distribution is softer for smaller m_{h_2} for $m_{h_2} > 2m_\chi$. On the other hand, when $m_{h_2} < 2m_\chi$, the DM pair can only be produced through off-shell h_2 mediation. Then the relative suppression on event rates with higher $m_{\chi\bar{\chi}}$ is weaker for lighter h_2 , leading to harder $p_T^{\chi\bar{\chi}}$ spectra for lighter h_2 . This can be seen from Fig. 13: For $m_{h_2} < 180$ GeV, the $p_T^{\chi\bar{\chi}}$ spectrum decreases with m_{h_2} . On the other hand, for $m_{h_2} > 180$ GeV, $p_T^{\chi\bar{\chi}}$ gets increased for larger m_{h_2} .

Finally, we show the upper limits on μ for Case C and Case D in the inclusive hadronic and semileptonic channels with the integrated luminosity of 36 fb^{-1} in Fig. 14. Due to

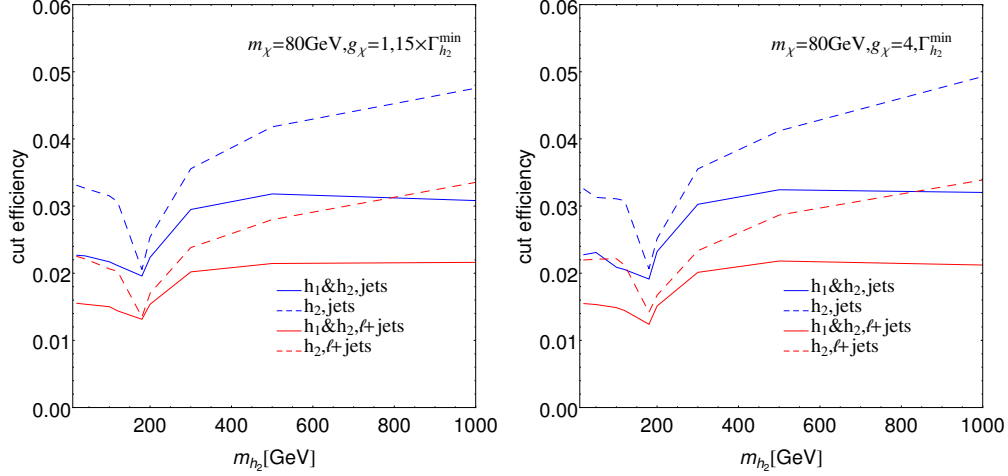


FIG. 12: Cut efficiencies for Case C and Case D in the SFDM model and simplified model in the inclusive hadronic (jets) and semileptonic (ℓ +jets) channels.

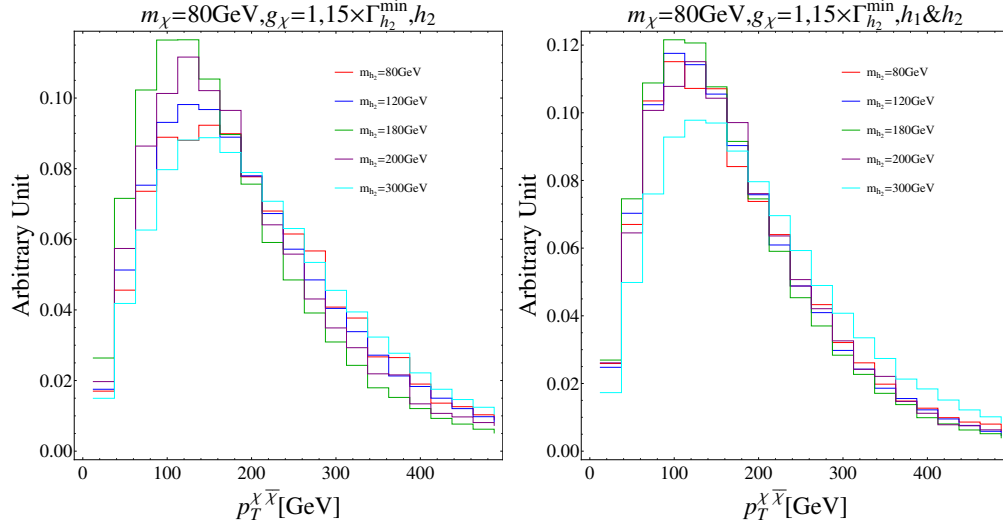


FIG. 13: The parton-level distributions of $p_T^{\chi\bar{\chi}}$ for Case C and Case D with mediator h_2 (left) and two mediators h_1 and h_2 (right) for different m_{h_2} .

the destructive interference between diagrams with h_1 and h_2 mediation, the LHC search sensitivities on the SFDM model are extremely weak in the region of $m_{h_2} < 2m_\chi$. Without the destructive interference effects as in the simplified model, the sensitivities in the same region can be more than order of magnitude better, but still way below the LHC probe at the current stage. For $m_{h_2} \gtrsim 2m_\chi$, the interference effects on the total cross section can be destructive or constructive in the SFDM model depending on m_{h_2} as shown in the right panel of Fig. 8. However, the interference effects always reduce the cut efficiency due to

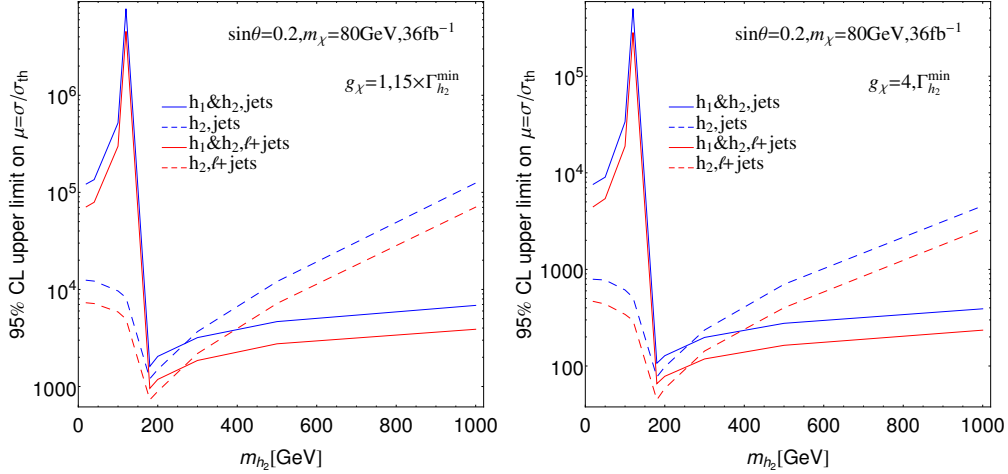


FIG. 14: The 95% C.L. upper limits on μ in the inclusive hadronic (jets) and semileptonic ($\ell + \text{jets}$) channels [62, 63] for Case C and Case D in the SFDM model (solid curves) and simplified model (dashed curves).

the softened energy scale as compared to that in the simplified model. Both facts lead to a better sensitivity in the SFDM model than that in the simplified model for $m_{h_2} \gtrsim 300$ GeV, and becomes opposite for $m_{h_2} \lesssim 300$ GeV.

V. SUMMARY

In this work, we have studied the impact of the 125 GeV Higgs boson on searches for DM in association with a top pair (DM+ $t\bar{t}$) at the LHC in the SFDM model with the Higgs portal. Depending on the mass relations of two mediators and the DM, four cases are considered. For Case A and Case B where the 125 GeV Higgs boson h_1 is on-shell, the DM production is dominated by the mediator h_1 . For Case C and Case D, h_1 is always off-shell while the mediator h_2 can be either on-shell or off-shell. The impact of h_1 is significant in certain parameter space in these cases, and the simplified model is not good enough.

Specifically, we find that when both h_1 and h_2 are off-shell (Case D), the destructive interference makes the total cross section much smaller than that in the simplified model without h_2 . If only h_2 is on-shell (Case C), the effect of h_1 on the total cross section becomes more important for larger m_{h_2} . Besides, with a larger total width of h_2 , which may come from a large coupling g_χ or dominant decay of h_2 into the extra dark sector particles, the relative contribution of h_1 (h_2) to the total cross section for Case C is further increased

(decreased). It is found that irrespective of g_χ and Γ_{h_2} the interference effect for Case C is destructive in the region of $2m_\chi \lesssim m_{h_2} \lesssim 380$ GeV and constructive for $m_{h_2} \gtrsim 380$ GeV with $\sin\theta = 0.2$ and $m_\chi = 80$ GeV. In addition to the total cross section, h_1 can also affect the differential distribution of the $\text{DM}+t\bar{t}$ process. Especially, the $p_T^{\chi\bar{\chi}}$ in the SFDM model is always softer as compared to that in the simplified model for Case C and Case D.

Finally, we study the impact of h_1 on the LHC bounds of the $\text{DM}+t\bar{t}$ search in the inclusive hadronic and semileptonic channels with the integrated luminosity of 36 fb^{-1} . We find that the upper limit on the signal strength μ for Case A in the SFDM model is smaller than 10, which is almost independent of m_{h_2} . For Case B, the sensitivity also depends on the triple scalar coupling λ_1 of $h_1 - h_2 - h_2$. Roughly, the upper limit is below 50 for the benchmark values discussed. For Case C, the sensitivity in the SFDM model is extremely weak as compared to that in the simplified model due to the destructive interference between the SM Higgs boson and the singlet scalar, which were largely ignored in theoretical and experimental papers except in Refs. [17, 26, 27, 31, 39, 40, 55]. For Case D, the upper limit in the SFDM model is better than that in the simplified model in the region of $m_{h_2} \gtrsim 300$ GeV and becomes opposite for $m_{h_2} \lesssim 300$ GeV.

Before closing, we would like to point out that the 125 GeV Higgs boson is also important for the VDM search at high-energy colliders. If one generates the vector DM mass by a dark Higgs mechanism, then there will be a mixing between the dark Higgs boson and the SM Higgs boson [25], resulting in two scalar propagators that can produce interesting interference [26, 27].⁸ Then the amplitude for the VDM pair production at high-energy colliders will take a form similar to Eq. (3.1). Effects of these two scalar propagators have been studied in the context of characterizing the mass and the spin of the Higgs portal scalar, fermion and vector DM at the ILC [39, 40] and at the LHC and 100 TeV pp collider [17].

In conclusion, we would like to emphasize that the contribution of the 125 GeV Higgs boson should be properly included to interpret correctly the LHC dark matter searches in case of the s -channel scalar mediators: It is important not only for the gauge invariance and renormalizability at the high-energy scale, but also for the quantitative difference of the upper limits and kinematic distributions.

⁸ Note that there is no need to consider two scalar propagators in case of real singlet scalar DM (see, for example, Ref. [39]).

ACKNOWLEDGMENTS

We would like to thank Cheng-Wei Chiang, Jiayin Gu, Jusak Tandean and Yi-Lei Tang for valuable discussions. GL is grateful to the KIAS members for kind hospitality. This work is supported in part the MOST MOST106-2112-M-002-003-MY3 (GL), by National Research Foundation of Korea (NRF) Research Grant NRF-2015R1A2A1A05001869 (PK, JL) and by the NRF grant funded by the Korea government (MSIP) (No. 2009-0083526) through Korea Neutrino Research Center at Seoul National University (PK).

Appendix A: Relic density and direct detection cross section

In this Appendix, we show the relic densities and spin-independent direct detection cross sections calculated using `micrOMEGAs` [71] for the benchmark points of the cases categorized in Section III.

Apart from the SM fermions or gauge bosons, the DM pair can also annihilate into scalar bosons if it is kinematically allowed. The couplings of $h_1 - h_2 - h_2$ and $h_2 - h_1 - h_1$ are defined in Eq. (2.19), while the couplings of $h_1 - h_1 - h_1$ and $h_2 - h_2 - h_2$ are given by

$$\lambda_{111} = \lambda_H v_H c_\theta^3 - \mu_1/2s_\theta c_\theta^2 + \lambda_{HS} v_H s_\theta^2 c_\theta - 1/6\mu_2 s_\theta^3, \quad (\text{A1})$$

$$\lambda_{222} = \lambda_H v_H s_\theta^3 + \mu_1/2c_\theta s_\theta^2 + \lambda_{HS} v_H c_\theta^2 s_\theta + 1/6\mu_2 c_\theta^3. \quad (\text{A2})$$

We take $\lambda_{HS} = 0.02$ and $\mu_2 = 100$ GeV so that the triple scalar couplings satisfy the experimental measurements. For instance, if $m_{h_2} = 80$ GeV, $\lambda_{111} = 0.94\lambda_{\text{SM}}$, $\lambda_{122} = -0.097\lambda_{\text{SM}}$, $\lambda_{211} = 0.44\lambda_{\text{SM}}$ and $\lambda_{222} = 0.52\lambda_{\text{SM}}$ with λ_{SM} defined in Eq. (2.22).

For Case C and Case D, a large coupling g_χ is allowed since $m_{h_1} < 2m_\chi$. As a result, the relic density of χ is small and can be below the measured DM relic density ($\Omega_0 h^2 = 0.120 \pm 0.001$) [72]. In Tab. I and Tab. II, we show the relic densities and direct detection cross sections for the benchmark points with $s_\theta = 0.2$, $g_\chi = 4$, $m_\chi = 80$ GeV and $m_{H_2} \in [70, 500]$ GeV. In Case C, the DM is annihilated away through the s -channel $h_{1,2}$ mediation. Given a large $g_\chi = 4$, the relic densities of all the benchmark points are below the measured DM relic density and are independent of the triple scalar couplings. In Case D, the relic densities for $m_{h_2} = 70$ and 90 GeV are far below the measured DM relic density due to the annihilation of $\chi\bar{\chi} \rightarrow h_2 h_2$. This channel is kinematically suppressed for $m_{h_2} \gtrsim 90$ GeV.

Then, the DM can only annihilate through the s -channel $h_{1,2}$ mediation as in Case C. For $m_{h_2} = 110$ and 130 GeV, the relic densities becomes much larger because of the cancellation between the contributions from the mediators h_1 and h_2 .

For Case A and Case B, since $m_{h_1} > 2m_\chi$ the coupling g_χ is severely constrained by the measurements of Higgs invisible decay branching ratio. In Tab. III, we show the relic densities for benchmark points in Case B with $g_\chi = 0.15$ and $m_\chi = 50$ GeV (the relic densities for Case A, which are larger, are not shown here). The relic densities of all benchmark points are larger than the measured DM relic density. As we explained in Section II, this can be weakened with the opening of new DM annihilation channels such as $\chi\bar{\chi} \rightarrow Z'Z'$ or coannihilation within a richer dark sector.

We can find that the DM-nucleon scattering cross section is well described by

$$\sigma_p^{\text{SI}} \propto (g_\chi \sin(2\theta))^2 \left(\frac{1}{m_{h_1}^2} - \frac{1}{m_{h_2}^2} \right)^2. \quad (\text{A3})$$

Benchmark points in all case are challenged by current DM direct detections [73–76] (for comparison, the σ_p^{SI} of points with $\Omega h^2 < 0.120$ should be rescaled by a factor $\Omega h^2/0.120$). This indicates that there will be other DM annihilation mechanisms if our DM indeed comprises a component of a full DM sector.

TABLE I: Relic densities and spin-independent direct detection cross sections for Case C with $s_\theta = 0.2$, $g_\chi = 4$ and $m_\chi = 80$ GeV.

m_{h_2} [GeV]	200	300	400	500
Ωh^2	2.56×10^{-2}	7.03×10^{-2}	8.51×10^{-2}	9.19×10^{-2}
σ_p^{SI} [pb]	1.30×10^{-7}	2.38×10^{-7}	2.84×10^{-7}	3.07×10^{-7}

TABLE II: Relic densities and spin-independent direct detection cross sections for Case D with $s_\theta = 0.2$, $g_\chi = 4$, $m_\chi = 80$ GeV, $\lambda_{HS} = 0.02$ and $\mu_2 = 100$ GeV.

m_{h_2} [GeV]	70	90	110	130	150
Ωh^2	1.87×10^{-5}	8.04×10^{-3}	1.15	3.72	3.72×10^{-2}
σ_p^{SI} [pb]	1.67×10^{-6}	3.01×10^{-7}	2.96×10^{-8}	1.99×10^{-9}	3.26×10^{-8}

TABLE III: Relic densities and spin-independent direct detection cross sections for Case B with $s_\theta = 0.2$, $g_\chi = 0.15$, $m_\chi = 50$ GeV, $\lambda_{HS} = 0.02$ and $\mu_2 = 100$ GeV.

m_{h_2} [GeV]	60	70	80	90
Ωh^2	8.27	8.31	8.17	7.77
σ_p^{SI} [pb]	5.40×10^{-9}	2.32×10^{-9}	1.01×10^{-9}	4.18×10^{-10}

-
- [1] M. R. Buckley, D. Feld, and D. Goncalves, Phys. Rev. **D91**, 015017 (2015), arXiv:1410.6497 [hep-ph].
- [2] U. Haisch and E. Re, JHEP **06**, 078 (2015), arXiv:1503.00691 [hep-ph].
- [3] J. Abdallah *et al.*, Phys. Dark Univ. **9-10**, 8 (2015), arXiv:1506.03116 [hep-ph].
- [4] D. Abercrombie *et al.*, (2015), arXiv:1507.00966 [hep-ex].
- [5] O. Buchmueller, M. J. Dolan, and C. McCabe, JHEP **01**, 025 (2014), arXiv:1308.6799 [hep-ph].
- [6] G. Busoni, A. De Simone, E. Morgante, and A. Riotto, Phys. Lett. **B728**, 412 (2014), arXiv:1307.2253 [hep-ph].
- [7] G. Busoni, A. De Simone, J. Gramling, E. Morgante, and A. Riotto, JCAP **1406**, 060 (2014), arXiv:1402.1275 [hep-ph].
- [8] G. Busoni, A. De Simone, T. Jacques, E. Morgante, and A. Riotto, JCAP **1409**, 022 (2014), arXiv:1405.3101 [hep-ph].
- [9] F. Pobbe, A. Wulzer, and M. Zanetti, JHEP **08**, 074 (2017), arXiv:1704.00736 [hep-ph].
- [10] C. Arina *et al.*, JHEP **11**, 111 (2016), arXiv:1605.09242 [hep-ph].
- [11] P. Harris, V. V. Khoze, M. Spannowsky, and C. Williams, Phys. Rev. **D91**, 055009 (2015), arXiv:1411.0535 [hep-ph].
- [12] P. Harris, V. V. Khoze, M. Spannowsky, and C. Williams, Phys. Rev. **D93**, 054030 (2016), arXiv:1509.02904 [hep-ph].
- [13] D. Pinna, A. Zucchetta, M. R. Buckley, and F. Canelli, (2017), arXiv:1701.05195 [hep-ph].
- [14] T. Plehn, J. Thompson, and S. Westhoff, (2017), arXiv:1712.08065 [hep-ph].
- [15] U. Haisch, P. Pani, and G. Polesello, JHEP **02**, 131 (2017), arXiv:1611.09841 [hep-ph].

- [16] M. R. Buckley and D. Goncalves, Phys. Rev. **D93**, 034003 (2016), [Phys. Rev.D93,034003(2016)], arXiv:1511.06451 [hep-ph].
- [17] B. Dutta, T. Kamon, P. Ko, and J. Li, (2017), arXiv:1712.05123 [hep-ph].
- [18] A. M. Sirunyan *et al.* (CMS), JHEP **07**, 014 (2017), arXiv:1703.01651 [hep-ex].
- [19] M. Aaboud *et al.* (ATLAS), (2017), arXiv:1710.11412 [hep-ex].
- [20] A. M. Sirunyan *et al.* (CMS), (2017), arXiv:1711.00752 [hep-ex].
- [21] C. Collaboration (CMS), *Search for dark matter produced in association with a top quark pair at $\sqrt{s} = 13$ TeV*, Tech. Rep. CMS-PAS-EXO-16-049 (2018).
- [22] Y. G. Kim, K. Y. Lee, and S. Shin, JHEP **05**, 100 (2008), arXiv:0803.2932 [hep-ph].
- [23] S. Baek, P. Ko, and W.-I. Park, JHEP **02**, 047 (2012), arXiv:1112.1847 [hep-ph].
- [24] S. Baek, P. Ko, W.-I. Park, and E. Senaha, JHEP **11**, 116 (2012), arXiv:1209.4163 [hep-ph].
- [25] S. Baek, P. Ko, W.-I. Park, and E. Senaha, JHEP **05**, 036 (2013), arXiv:1212.2131 [hep-ph].
- [26] S. Baek, P. Ko, M. Park, W.-I. Park, and C. Yu, Phys. Lett. **B756**, 289 (2016), arXiv:1506.06556 [hep-ph].
- [27] P. Ko and J. Li, Phys. Lett. **B765**, 53 (2017), arXiv:1610.03997 [hep-ph].
- [28] A. Albert *et al.*, Phys. Dark Univ. **16**, 49 (2017), arXiv:1607.06680 [hep-ex].
- [29] C.-W. Chiang and E. Senaha, Phys. Lett. **B750**, 147 (2015), arXiv:1508.02891 [hep-ph].
- [30] D. McKeen, M. Pospelov, and A. Ritz, Phys. Rev. **D86**, 113004 (2012), arXiv:1208.4597 [hep-ph].
- [31] S. Choi, S. Jung, and P. Ko, JHEP **10**, 225 (2013), arXiv:1307.3948 [hep-ph].
- [32] S. Esch, M. Klasen, and C. E. Yaguna, Phys. Rev. **D88**, 075017 (2013), arXiv:1308.0951 [hep-ph].
- [33] M. Fairbairn and R. Hogan, JHEP **09**, 022 (2013), arXiv:1305.3452 [hep-ph].
- [34] T. Robens and T. Stefaniak, Eur. Phys. J. **C76**, 268 (2016), arXiv:1601.07880 [hep-ph].
- [35] D. O’Connell, M. J. Ramsey-Musolf, and M. B. Wise, Phys. Rev. **D75**, 037701 (2007), arXiv:hep-ph/0611014 [hep-ph].
- [36] J. M. No and M. Ramsey-Musolf, Phys. Rev. **D89**, 095031 (2014), arXiv:1310.6035 [hep-ph].
- [37] C.-Y. Chen, S. Dawson, and I. M. Lewis, Phys. Rev. **D91**, 035015 (2015), arXiv:1410.5488 [hep-ph].
- [38] I. M. Lewis and M. Sullivan, (2017), arXiv:1701.08774 [hep-ph].
- [39] P. Ko and H. Yokoya, JHEP **08**, 109 (2016), arXiv:1603.04737 [hep-ph].

- [40] T. Kamon, P. Ko, and J. Li, Eur. Phys. J. **C77**, 652 (2017), arXiv:1705.02149 [hep-ph].
- [41] G. Dupuis, JHEP **07**, 008 (2016), arXiv:1604.04552 [hep-ph].
- [42] T. Huang, J. M. No, L. Perni, M. Ramsey-Musolf, A. Safonov, M. Spannowsky, and P. Winslow, (2017), arXiv:1701.04442 [hep-ph].
- [43] A. Falkowski, C. Gross, and O. Lebedev, JHEP **05**, 057 (2015), arXiv:1502.01361 [hep-ph].
- [44] J. R. Andersen *et al.* (LHC Higgs Cross Section Working Group), (2013), 10.5170/CERN-2013-004, arXiv:1307.1347 [hep-ph].
- [45] F. Maltoni, K. Paul, T. Stelzer, and S. Willenbrock, Phys. Rev. **D64**, 094023 (2001), arXiv:hep-ph/0106293 [hep-ph].
- [46] G. Aad *et al.* (ATLAS), JHEP **11**, 206 (2015), arXiv:1509.00672 [hep-ex].
- [47] G. Aad *et al.* (ATLAS, CMS), JHEP **08**, 045 (2016), arXiv:1606.02266 [hep-ex].
- [48] V. Khachatryan *et al.* (CMS), JHEP **10**, 144 (2015), arXiv:1504.00936 [hep-ex].
- [49] G. Aad *et al.* (ATLAS), Eur. Phys. J. **C76**, 45 (2016), arXiv:1507.05930 [hep-ex].
- [50] ATLAS Collaboration, Tech. Rep. ATLAS-CONF-2017-058 (2017).
- [51] V. Khachatryan *et al.* (CMS), JHEP **02**, 135 (2017), arXiv:1610.09218 [hep-ex].
- [52] C. Collaboration (CMS), *Search for invisible decays of the Higgs boson produced through vector boson fusion at $\sqrt{s} = 13$ TeV*, Tech. Rep. CMS-PAS-HIG-17-023 (2018).
- [53] V. Khachatryan *et al.* (CMS), JHEP **09**, 051 (2016), arXiv:1605.02329 [hep-ex].
- [54] V. Khachatryan *et al.* (CMS), JHEP **10**, 076 (2017), arXiv:1701.02032 [hep-ex].
- [55] S. Baek, P. Ko, and J. Li, Phys. Rev. **D95**, 075011 (2017), arXiv:1701.04131 [hep-ph].
- [56] C. Collaboration (CMS), *Combination of searches for Higgs boson pair production in proton-proton collisions at $\sqrt{s} = 13$ TeV*, Tech. Rep. CMS-PAS-HIG-17-030 (2018).
- [57] D. E. Brahm and L. J. Hall, Phys. Rev. **D41**, 1067 (1990).
- [58] P. Ko and Y. Tang, JCAP **1405**, 047 (2014), arXiv:1402.6449 [hep-ph].
- [59] P. Ko, Y. Omura, and C. Yu, JHEP **11**, 054 (2014), arXiv:1405.2138 [hep-ph].
- [60] S. Baek, P. Ko, and W.-I. Park, Phys. Lett. **B747**, 255 (2015), arXiv:1407.6588 [hep-ph].
- [61] K. Griest and D. Seckel, Phys. Rev. **D43**, 3191 (1991).
- [62] CMS Collaboration, Tech. Rep. CMS-PAS-EXO-16-005 (2016).
- [63] A. M. Sirunyan *et al.* (CMS), (2017), arXiv:1706.02581 [hep-ex].
- [64] J. Alwall, R. Frederix, S. Frixione, V. Hirschi, F. Maltoni, O. Mattelaer, H. S. Shao, T. Stelzer, P. Torrielli, and M. Zaro, JHEP **07**, 079 (2014), arXiv:1405.0301 [hep-ph].

- [65] T. Sjostrand, S. Mrenna, and P. Z. Skands, JHEP **05**, 026 (2006), arXiv:hep-ph/0603175 [hep-ph].
- [66] J. de Favereau, C. Delaere, P. Demin, A. Giammanco, V. Lematre, A. Mertens, and M. Selvaggi (DELPHES 3), JHEP **02**, 057 (2014), arXiv:1307.6346 [hep-ex].
- [67] M. Cacciari, G. P. Salam, and G. Soyez, Eur. Phys. J. **C72**, 1896 (2012), arXiv:1111.6097 [hep-ph].
- [68] A. L. Read, J. Phys. **G28**, 2693 (2002).
- [69] T. Junk, Nucl. Instrum. Meth. **A434**, 435 (1999), arXiv:hep-ex/9902006 [hep-ex].
- [70] G. Cowan, K. Cranmer, E. Gross, and O. Vitells, Eur. Phys. J. **C71**, 1554 (2011), [Erratum: Eur. Phys. J. C73,2501(2013)], arXiv:1007.1727 [physics.data-an].
- [71] G. Belanger, F. Boudjema, A. Pukhov, and A. Semenov, Comput. Phys. Commun. **180**, 747 (2009), arXiv:0803.2360 [hep-ph].
- [72] N. Aghanim *et al.* (Planck), (2018), arXiv:1807.06209 [astro-ph.CO].
- [73] D. S. Akerib *et al.* (LUX), Phys. Rev. Lett. **118**, 021303 (2017), arXiv:1608.07648 [astro-ph.CO].
- [74] E. Aprile *et al.* (XENON), (2017), arXiv:1705.06655 [astro-ph.CO].
- [75] X. Cui *et al.* (PandaX-II), (2017), arXiv:1708.06917 [astro-ph.CO].
- [76] E. Aprile *et al.* (XENON), (2018), arXiv:1805.12562 [astro-ph.CO].